Combustion and Flame 276 (2025) 114144

Contents lists available at ScienceDirect

Combustion and Flame

journal homepage: www.sciencedirect.com/journal/combustion-and-flame

# Theoretical study of the real-fluid laminar flame propagation under supercritical conditions by using the virial equation of state and the Enskog transport model

Junfeng Bai, Xin Zhang, Hao Zhao *

*College of Engineering, Peking University, Beijing 100871, PR China*

ARTICLE INFO

*Keywords:*
Real fluid
Transport properties
Virial equation of state
Enskog transport model
Supercritical modelling

ABSTRACT

A real-fluid computation model using the Virial equation of state and the Enskog transport model was developed in this work to simulate real-fluid laminar flame propagations, and it was also compared with the Redlich-Kwong-Ely-Hanley/Takahashi real-fluid model in literature. The real-fluid effects of equation of state, thermodynamics, chemical potential, thermal conductivity, and mass diffusion have been investigated on the freely propagating flame simulations of different fuels. The contribution and the source of uncertainties by different real-fluid properties are also comprehensively discussed. The overall effects of real-fluid behaviors on the laminar flame speed simulations in $H_2O$-dilute mixtures can reach 35 % at 100 atm, which reveal that accurate descriptions of real-fluid effects are crucial for flame speed predictions, especially using dilute gas with a high polarization, such as $H_2O$. The Redlich-Kwong-Ely-Hanley/Takahashi model shows severe over-predictions of the hydrogen laminar flame speeds due to its significant weakness in predictions of thermal conductivities of mixtures by comparing with the NIST data, while the present Virial-Enskog model exhibits more reasonable predictability. The real-fluid simulations of the laminar flame speeds of DME and n-heptane flames by using the Virial-Enskog model and the Redlich-Kwong-Ely-Hanley/Takahashi model are compared with the available experimental data. It shows a crucial real-fluid effect on the simulations of DME and n-heptane flame speeds, up to 8 % discrepancy from the ideal-gas flame speed prediction, even at 20–25 atm. Overall, the Virial-Enskog model provides better estimations of the real-fluid behaviors than the empirical Redlich-Kwong-Ely-Hanley/Takahashi model, especially at high pressures.

**Novelty and significance statement**

The novelty of this combustion simulation study is the development of a real-fluid computation model using the Virial equation of state (EoS) and the Enskog transport model to simulate real-fluid laminar flame propagations. It includes deeper-level physical insights compared with the RK-EH/Takahashi real-fluid model in the literature. The real-fluid effects of EoS, thermodynamics, chemical potential, thermal conductivity, and mass diffusion have been investigated on the freely propagating flame simulations of different fuels, respectively. The contribution and the source of uncertainties by different real-fluid properties are comprehensively discussed. The Virial-Enskog model provides better estimations of the real-fluid behaviors than the empirical RK-EH/Takahashi model, especially at high pressures.

## 1. Introduction

To achieve lower emissions and higher thermodynamic efficiency, the supercritical combustion strategy at high pressures is drawing increasing attention in the design of advanced internal combustion engines and rocket engines [1–4]. Its distinct features are that the pressure is generally above 100 atm, and most of the reactants and products are in the supercritical phase [5,6]. The traditional ideal-gas reaction kinetics theory is not applicable to the study of supercritical combustion in engines, where the intermolecular force is not negligible, and the molecular collision cross section and the collision frequency are generally different from ideal-gas parameters [7]. Therefore, species density, thermodynamic properties, and transport properties need to be

* Corresponding author.
*E-mail address:* h.zhao@pku.edu.cn (H. Zhao).

https://doi.org/10.1016/j.combustflame.2025.114144
Received 4 November 2024; Received in revised form 24 March 2025; Accepted 25 March 2025
Available online 1 April 2025

computed by considering the real-fluid effects. For example, the real-fluid heat capacity of water at 100 atm and 800 K is 20 % higher than the corresponding ideal-gas state value [8], potentially resulting in a 20 % difference in the adiabatic flame temperature predictions.

A computation code for real-fluid thermodynamics using the Virial equation of state (EoS) has been developed and validated in our previous work on the 0-D real-fluid simulations [8,9]. The Virial method can provide more accurate and convenient evaluations of real-fluid compressibility, thermodynamics, and chemical potential computations than the empirical Redlich-Kwong (RK) EoS method [10,11] under supercritical conditions for universal fuels. However, the real-fluid transport properties have not been computed, and their effects on the 1-D real-fluid flame simulations have not been studied.

The rigorous kinetic theory of dilute fluids proposed by Chapman and Enskog [12] was adopted in the conventional calculation method of transport parameters [13,14]. It assumes that there are only two-body collisions and the molecular volume is ignorable. These assumptions are valid in dilute fluids while creating distinct errors in dense fluids, such as the supercritical fluid, where molecular structures and multi-body interactions are non-negligible. To further describe the pressure dependence of the transport properties in dense fluids, both empirical and theoretical models were developed in the literature.

The empirical models were generally fitted with experimental data of species transport at varied pressures, which lacks of physical insights on real-fluid intermolecular interactions. Moreover, experimental measurements of species' thermal and mass diffusivities against pressure are very limited and have large uncertainties, especially for radicals and complex molecules at high pressures. Generally, researchers utilize measured transport properties of known molecules to predict the transport parameters of similar molecules and radicals based on critical properties, which is named the principle of corresponding states [15]. Ely and Hanley [15] reported the fitting formula of thermal conductivities of pure substances and mixtures based on the principle of corresponding states referring to the experimental data of methane. The predicted data was compared with experimental data of dozens of pure substances and mixtures. The prediction error of thermal conductivity is up to 20 % at low temperatures and high pressures. Takahashi [16] reported a generalized chart for the corrections of self- and binary-diffusion coefficients of mass at high pressures based on the principle of corresponding states. Based on the experimental fitting method of transport properties, Liang et al. [17] studied the effects of real-fluid transport properties on laminar flame speeds at high pressures by simulating laminar flame propagations in supercritical hydrogen/air and methane/air mixtures. The methods of Ely and Hanley (EH) and Takahashi were employed in the calculations of thermal conductivities and self-/binary-diffusion coefficients, respectively. However, the laminar flame speeds in supercritical hydrogen/air mixtures decrease with including the real-fluid thermal conductivities according to their work, which is not physical. That is because the thermal conductivities increase due to the real-fluid interactions according to the experimental data in NIST database [18], resulting in an increase of laminar flame speeds accordingly [19]. Gopal et al. [20] investigated the real fluid effects in cryogenic laminar premixed $CH_4$–$O_2$ flames using the Peng-Robinson (PR) EoS and the Chung [21] and Takahashi [16] empirical correlations for real fluid transport properties. The real fluid flame speed is smaller than the ideal gas by a factor of about 5 in their simulations at 140K. Terashima et al. [22] studied propagating flames under high-pressure conditions with real-fluid combustion modeling using the Soave-Redlich-Kwong (SRK) EoS and the Chung [21] and Riazi/Whitson [23] empirical correlations for real fluid transport properties. The results demonstrate that the real-fluid consideration offers a better prediction accuracy for the negative pressure dependence of the mass burning rate in the $H_2/O_2$/Ar flame case compared to the ideal-gas model. However, the influence of density, thermodynamics, chemical potential, and transport properties on real-fluid flame computations has not been separately discussed in these studies. Giovangigli et al. [24] investigated a detailed high-pressure flame model and the structure of planar transcritical $H_2$–$O_2$–$N_2$ flames, and performed a sensitivity analysis with respect to the model's parameters. The Soave–Redlich–Kwong EoS was employed and the transport coefficients were obtained by using Stefan–Maxwell equations derived from the kinetic theory of dense gases or from experiments in fluids. Weng et al. [25] investigated on the dynamics of adiabatic and nonadiabatic spherically expanding laminar flame using the Noble-Abel EoS. The effect of the finite molecular volume was considered and characterized by a covolume parameter. Zhang et al. [26] simulated the propagation of laminar oxy-syngas and oxy-methane flames diluted by supercritical carbon dioxide. The real fluid models were considered for the equation of state, thermodynamic functions, transport properties, as well as the mass action law using the Redlich-Kwong EoS. The Chung's model [21] revised by Gopal et al. [20] was used for thermal conductivity calculation while Takahashi's model [16] was adopted for binary diffusion coefficient. Lv et al. [27] comprehensively evaluated real-fluid effects on laminar premixed $H_2/O_2$ flames under cryogenic and high-pressure conditions by using the Peng–Robinson EoS. This work highlights the significance of the correction of transport properties for predicting flame thickness.

Enskog first developed a kinetic theory of dense fluids made up of rigid spherical molecules [13,14]. Due to the non-ignorable molecular volume in this special model, the increased collisional transfer of momentum and energy and collisional frequency need to be accurately described. The correction factors of transport properties were derived based on the modified Boltzmann equation. Although the derivations were obtained for fluids made up of rigid spherical molecules, Enskog also reported that these corrections can be applied to real fluids by introducing the "thermal pressure" [13,14]. Therefore, the Enskog model includes physical insights in the statistic mechanics level, and exhibits the potential for improved accuracy comparing with the empirical models, especially for large molecules and radicals. However, the Enskog model has not been applied for real-fluid simulations, even though it has been developed for years. That is because it needs to be employed based on the realization of the Virial equation of state (EoS). Fortunately, we have developed and applied the Virial EoS source code in cantera for 0-D real-fluid simulations in our recent works [8,9], and then we apply the Enskog model for theoretical computations of pressure-dependent real-fluid transport properties and for 1-D flame simulations in this work.

Here, the computation code for real fluids by using the Virial EoS and the Enskog transport model was developed as the theoretical Virial-Enskog model and incorporated into the Cantera program [28]. The calculations of real-fluid transport properties have been coupled with the calculations of real-fluid EoS, thermodynamics properties, and chemical potentials to realize the 1-D simulations by using the Virial-Enskog model at high pressures. Its predictivity was also compared with the empirical RK-EH/Takahashi model, which was comprised of the RK EoS and the EH/Takahashi transport model. The real-fluid effects on compressibility factors, thermodynamic properties, chemical potentials, and transport properties for the laminar flame simulations in different supercritical mixtures have been discussed respectively. The laminar flame speed results simulated by using the real-fluid methods were also compared with the available experimental data in the literature.

## 2. Theoretical methods

For the 1-D flow problem with chemical reactions, the governing conservation equations are reduced to:

$$\dot{M}\frac{dT}{dx}-\frac{1}{c_p}\frac{d}{dx}\left(\lambda A\frac{dT}{dx}\right)+\frac{A}{c_p}\sum_{k=1}^{K}\rho Y_k V_k c_{pk}\frac{dT}{dx}+\frac{A}{c_p}\sum_{k=1}^{K}\dot{\omega}_k h_k W_k=0 \qquad (1)$$

$$\dot{M}\frac{dY_k}{dx}+\frac{d}{dx}(\rho A Y_k V_k)-A\dot{\omega}_k W_k=0\ (k=1,\ldots,\mathrm{K}) \tag{2}$$

where $\dot{M}=\rho uA$ is the mass flow rate; $\rho$ is the mass density; $u$ is the velocity of the mixture; $A$ is the cross-sectional area; $T$ is the temperature; $x$ is the 1-D coordinate; $c_p$ and $c_{pk}$ are the constant-pressure heat capacity of the mixture and the $k$-th species; $\lambda$ is the thermal conductivity; $Y_k$ and $V_k$ are the mass fraction and mass diffusion velocity of the $k$-th species; $\dot{\omega}_k$, $h_k$,$W_k$ are the molar rate of production by chemical reaction per unit volume; the specific enthalpy; and the molecular weight of the $k$-th species.

To account for the real-fluid behaviors in the 1-D simulations, the density $\rho$ was calculated using the RK EoS and the Virial EoS, the total enthalpy, the total heat capacity, and the rate of production was calculated based on the RK method and the Virial method. The Virial method and the RK method have been described comprehensively in our previous work on the 0-D real-fluid simulations [8,9]. The Virial EoS [13] was used to describe real-fluid behaviors in the Virial method:

$$\frac{p\widetilde{V}}{RT}=1+\frac{B(T)}{\widetilde{V}} \tag{3}$$

where the coefficient $B(T)$ is called the second Virial coefficient, representing the correction of real-fluid effects [29]; $p$, $\widetilde{V}$ are pressure and molar volume; $R$ is the ideal-gas constant. Real-fluid partition function with Lennard-Jones (L-J) (6–12) potential [30] and Stockmayer potential [31,32] models were used to derive the expressions of Virial coefficients.

The RK EoS [10,11] is:

$$p=\frac{RT}{\widetilde{V}-b}-\frac{a}{\widetilde{V}\sqrt{T}(\widetilde{V}+b)} \tag{4}$$

where the parameters $a$ and $b$, accounting for the real-fluid behaviors, are calculated by using critical properties. The corrections of real-fluid thermodynamics and chemical potentials [33] were also derived based on the Virial EoS and the RK EoS to realize the complete Virial method and RK method. The species activity $\alpha_i$ is influenced by a function of chemical potential $\mu_i$ for real fluids and $\mu_i^0$ for ideal fluids [33]:

$$\alpha_i=\exp\left(\frac{\mu_i-\mu_i^0}{RT}\right) \tag{5}$$

The relationship between activity $\alpha$ and fugacity $f$ can be represented as:

$$\alpha=\frac{f}{f^o} \tag{6}$$

where $f^o$ is the fugacity at standard state (usually 1 atm or pressure under other standard conditions).

All the codes above have been realized, validated, and incorporated into the Cantera program [28] in our previous work [8,9]. However, the corrections of the partial molar enthalpy, the partial molar heat capacity, the thermal conductivity, and the mass diffusion need to be derived and coupled with the 0-D real-fluid simulation code in this work to fully realize the real-fluid 1-D simulations.

First, the partial molar enthalpy $h_k$ and the partial molar heat capacity $c_{pk}$ were computed by taking the derivative of the total enthalpy $h$ and the total heat capacity $c_p$ with respect to the molecular number of species $n_k$:

$$c_{pk}=\left(\frac{\partial c_p}{\partial n_k}\right)_{T,V} \tag{7}$$

$$h_k=\left(\frac{\partial h}{\partial n_k}\right)_{T,V} \tag{8}$$

where $V$ is the volume. The partial molar enthalpy $h_k$ and the partial molar heat capacity $c_{pk}$ were derived for both the Virial method and the RK method in this work.

The thermal conductivities and the mass diffusions were calculated by using both the EH/Takahashi model and the Enskog model. For the EH/Takahashi model, we used the calculation formula of the thermal conductivities at high pressures reported by Ely and Hanley. The principle of corresponding states was used to predict the thermal conductivities of all pure substances and mixtures by referring to the measured thermal conductivities of methane at different relative pressures $p_r=p/p_c$ and relative temperatures $T_r=T/T_c$, where $p$ and $T$ are the pressures and temperatures of the system, $p_c$ and $T_c$ are the critical pressures and critical temperatures.

The real-fluid mass diffusion was calculated by using the correction formula and chart derived by Takahashi. The correction formula is:

$$D/D^0=F_p\left(1-AT_r^{-B}\right)\left(1-CT_r^{-E}\right) \tag{9}$$

where $D/D^0$ is the total correction factor, $F_p$ presents the pressure corrections, while $\left(1-AT_r^{-B}\right)\left(1-CT_r^{-E}\right)$ presents the temperature corrections. The coefficients $F_p$, $A$, $B$, $C$, and $E$ can be sought from the correction chart using the relative pressures $p_r$ and relative temperatures $T_r$.

For the theoretical Enskog model, the correction factors of transport properties were derived based on the modified Boltzmann equation using rigid spherical molecules models and generalized to apply to real fluids. The correction formulas of the thermal conductivities $\lambda$ and the mass diffusions $D$ are:

$$\frac{\lambda\widetilde{V}}{\lambda^0 b_0}=\frac{1}{y}+1.2+0.755y \tag{10}$$

$$\frac{D\widetilde{V}}{D^0 b_0}=\frac{1}{y}+1 \tag{11}$$

where $b_0=B+T\frac{dB}{dT}$. $\lambda^0$ and $D^0$ are the ideal thermal conductivities and the ideal mass diffusions. $y$ is the correction factor given by

$$y=\frac{\widetilde{V}}{RT}\left[T\left(\frac{\partial p}{\partial T}\right)_{\widetilde{V}}\right]-1 \tag{12}$$

To describe real-fluid behaviors in fluid mixtures, a series of theoretical mixing rules [13] are applied for Virial coefficient calculations in this work. The second Virial coefficient $B_{mix}$ in mixtures is obtained as:

$$B_{mix}=\sum_i\sum_j X_i X_j B_{ij} \tag{13}$$

Where $X_i$ is mole fraction of $i$-th species. The interactive second Virial coefficient $B_{ij}$ is computed using corresponding interactive force constants. The similar mixing rules are used for transport models.

The multi-component model considering the Soret effect was used for all the calculations. The multicomponent diffusion coefficients, thermal conductivities, and thermal diffusion coefficients are computed from the solution of a system of equations defined by the so-called L matrix [34]. It is convenient to refer to the L matrix in terms of its nine block sub-matrices. The critical properties for radicals and intermediate species were estimated based on the critical properties for stable molecules. The inlet boundary condition of fuels was defined in velocity.

In 1-D simulations in Cantera, the width of the domain is set as 0.03 m, the initial grid is set as [0.0, 0.001, 0.01, 0.02, 0.029, 0.03], and the criteria used for grid refinement is set as (ratio=3, slope=0.02, curve=0.02), the number of points in domain is normally higher than 100.

This work mainly aims to construct the Virial-Enskog model. The RK-EH/Takahashi model is chosen for comparison since it has already partially applied in Cantera. RK and EH/Takahashi models were already realized and only some interfaces needed to be supplemented.

Therefore, we only compare the performance of the Virial-Enskog model with the RK-EH/Takahashi model in Cantera to avoid additional simulation uncertainties from using different programs.

## 3. Results and discussion

### 3.1. Hydrogen/air flames

The RK-EH/Takahashi model and the Virial-Enskog model were used to perform the simulations of the hydrogen laminar flame at 100 atm. The results are shown in Fig. 1. The chemical kinetics model reported by Burke et al. [35] was used in the simulations. To discuss the effects of real-fluid behaviors separately, the real-fluid EoS, thermodynamics, chemical potential, thermal conductivities, and mass diffusions were taken into account progressively. To be specific, Case 1 represents the simulations using the ideal gas treatment completely as a comparison. Cases 2–4 incorporate the corrections of the real-fluid EoS, thermodynamics, and chemical potential progressively using the RK EoS. Cases 5–6 incorporate the corrections of the real-fluid thermal conductivities and mass diffusions progressively using the EH/Takahashi model. Correspondingly, the simulations were performed using the Virial-Enskog model in Cases 7–11. Cases 7–9 consider the effects of the real-fluid EoS, thermodynamics, and chemical potential progressively using the Virial method. Cases 10–11 further incorporate the corrections of the real-fluid thermal conductivities and mass diffusions progressively using the Enskog model.

The laminar flame speed follows the scaling law:

$$S \propto \sqrt{\lambda/\rho c_p} \tag{14}$$

According to Fig. 1, the laminar flame speeds at different equivalence ratios increase using the RK EoS compared with using the ideal EoS. This is mainly caused by the change in mixture density. With the RK EoS, the density of the mixture decreases because the compressibility factors of hydrogen and nitrogen are over 1 [8]. However, the burning flux is almost unaffected. Since the laminar flame speeds are the burning flux divided by the density of the mixture, they increased using the RK EoS. From Case 2 to Case 3, the corrections of the total enthalpy $\boldsymbol{h}$ and heat capacity $\boldsymbol{c_p}$, the partial molar enthalpy $\boldsymbol{h_k}$ and heat capacity $\boldsymbol{c_{pk}}$ based on the RK EoS were further included. The major effect of real-fluid thermodynamics comes from the increase of heat capacity, which results in a decrease of system temperature in the simulations, hence the reactivity of the system is inhibited and the laminar flame speeds decrease.

The heat capacity comparisons for hydrogen/air mixture using different models are shown in Fig. 2. The real-fluid effects on heat capacity are important at 300 K to 1000K. The largest difference is up to 7 % at 300K. From Case 3 to Case 4, the correction of the real-fluid chemical potential based on the RK EoS was further considered. With this correction, species activity concentrations increase and then reaction rates are accelerated, which corresponds to faster oxidation of hydrogen in the real-fluid simulations. From Case 1 to Case 4, all the real-fluid behaviors based on the RK EoS were incorporated. From Case 4 to Case 5, the EH model was used for the real-fluid thermal conductivity calculations. The laminar flame speeds increase dramatically in Case 5. In the rigorous kinetics theory of dilute fluids, the thermal conductivities are independent of the pressures. However, in real dense fluids, the thermal conductivities increase with the increase of the pressure. Moreover, the laminar flame speeds increase with the increase of the thermal conductivities, therefore the laminar flame speeds increase using the EH model. From Case 5 to Case 6, the correction of real-fluid mass diffusions derived by Takahashi was used. The effects on the flame speeds are relatively small. This is mainly because the effects of real-fluid behaviors on the mass diffusions are small, which can cause

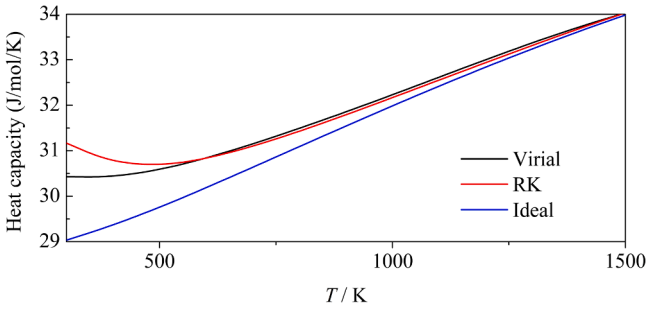


**Fig. 2.** The heat capacity comparisons for hydrogen/air mixture at 100 atm by using different models, φ=1.

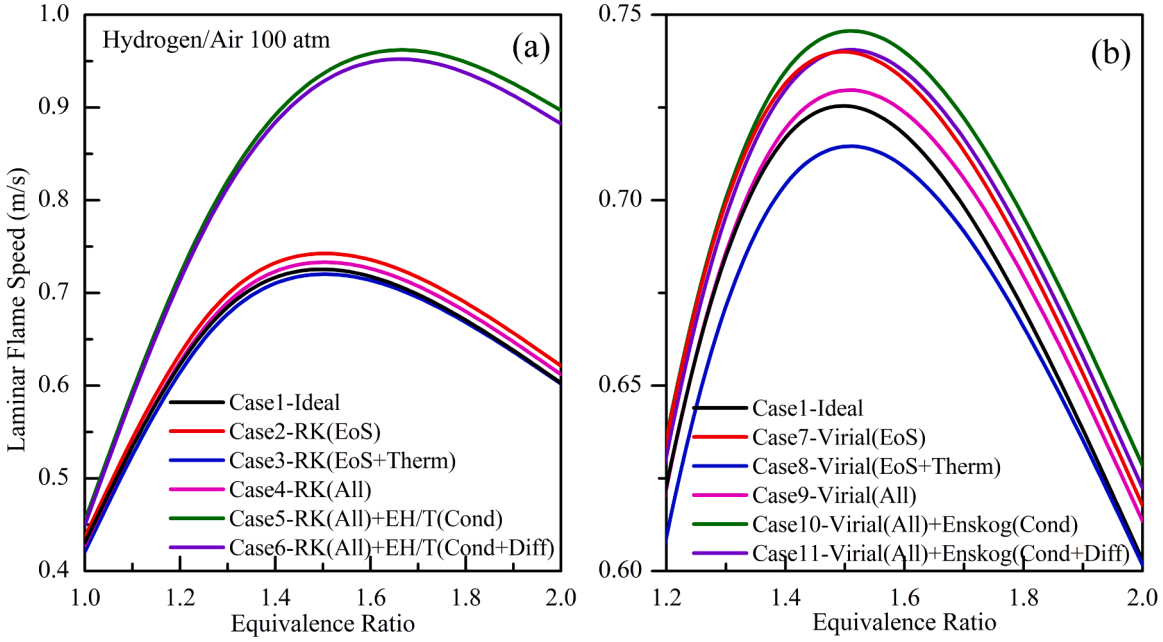


**Fig. 1.** The laminar flame speed simulations of hydrogen/air at 100 atm by using (a) the RK-EH/Takahashi and (b) the Virial-Enskog model. The initial temperature of the mixtures is $T_i$=298K.

within ±10 % deviation.

For Case 7–11 in Fig. 1, the simulations were performed by using the Virial-Enskog models. The effects of the real-fluid EoS, thermodynamics, and chemical potential using the Virial method were considered in Case 7–9. The laminar flame speeds increase considering the total effects of real-fluid behaviors based on the Virial method. The effects in Cases 7–9 using the Virial method are consistent with those using the RK method, namely Cases 2–4. Case 10 further incorporates the corrections of the real-fluid thermal conductivities using the Enskog model. Being consistent with the discussion for Case 5, the laminar flame speeds increase with the increase of the thermal conductivities in real dense fluids. However, the increment is much less.

To account for the big difference in the increment simulated by using the EH/Takahashi model and the Enskog model, the thermal conductivities of hydrogen, nitrogen, and oxygen computed by using both models were compared with the NIST data [18] and shown in Fig. 3. It can be observed that the thermal conductivities of hydrogen, nitrogen, and oxygen computed by using the Enskog model shows good agreement with the NIST data. However, the thermal conductivities computed by using the EH model show a larger deviation, especially at higher temperatures. This is the main reason that causes a dramatic increase in laminar flame speeds simulated by using the EH model. As discussed above, the principle of corresponding states was used to predict the thermal conductivities of all pure substances and mixtures by referring to the measured thermal conductivities of methane in the EH model. The deviation in Case 5 shows obvious limitations and uncertainties of the EH model. Moreover, the thermal conductivities of small molecules, such as $H_2$, $N_2$, and $O_2$ have not been calculated in the EH model, which potentially creates large errors in predicting the laminar flame speeds. Case 11 further incorporates the corrections of the real-fluid mass diffusions using the Enskog model. Consistent with the discussion for Case 6, the effects on the flame speeds are relatively small because the effects of real-fluid impacts on the mass diffusions are small.

The thermal diffusivities of hydrogen, nitrogen, and oxygen at 100 atm computed by using both models were compared with the NIST data [18] and shown in Fig. 4. It can be also observed that the thermal diffusivities of hydrogen, nitrogen, and oxygen computed by using the Virial-Enskog model shows good agreement with the NIST data.

The simulations of the $H_2/O_2/H_2O$ laminar flame at 100 atm at different equivalence ratios are shown in Fig. 5 and the analyses of the real-fluid effects based on these $H_2/O_2/H_2O$ cases are shown in Fig. 6. Different from fuel/air mixture, in $H_2/O_2/H_2O$ mixture, the molar ratio of $O_2$ and $H_2O$ is kept as 1:10 and the molar fraction of $H_2$ increase with the equivalence ratio increase. The laminar flame speeds are strongly inhibited considering real-fluid effects using both models. The main contribution is from the increase of real-fluid density and the increase of real-fluid heat capacity using $H_2O$ as dilute gas. From Case 4 to Case 5, considering the real-fluid thermal conductivities using the EH model, the laminar flame speeds decrease, which is contrary to our above discussions that the laminar flame speeds should increase with the increase of thermal conductivities considering real-fluid effects. This is because the real-fluid thermal conductivities of $H_2O$ calculated using the EH model are smaller than the ideal case. The comparisons of the thermal conductivities of water computed by using different models are shown in

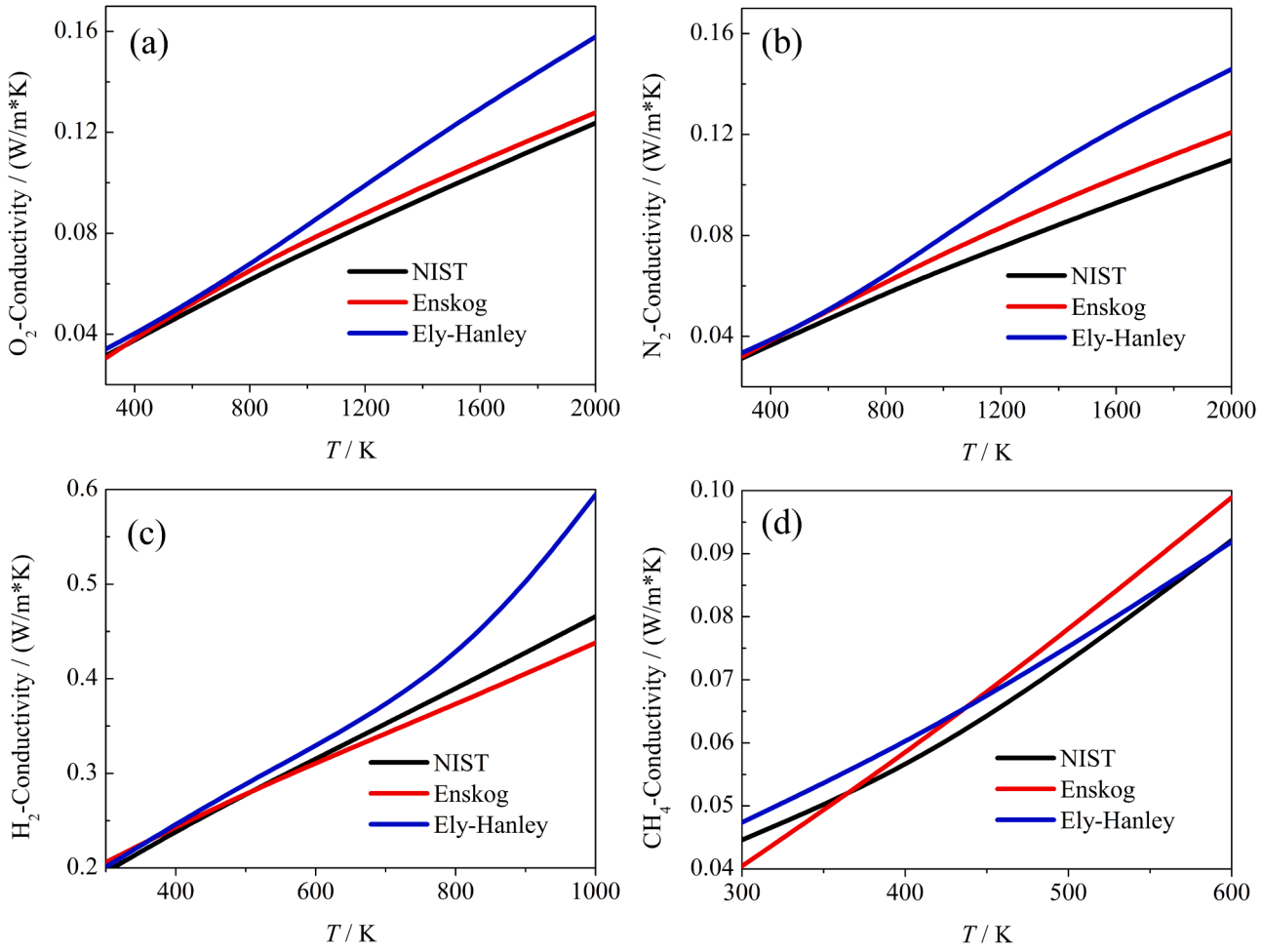


**Fig. 3.** The comparisons of the thermal conductivities of hydrogen, nitrogen, oxygen, and methane at 100 atm computed by using different models with the NIST data [18].

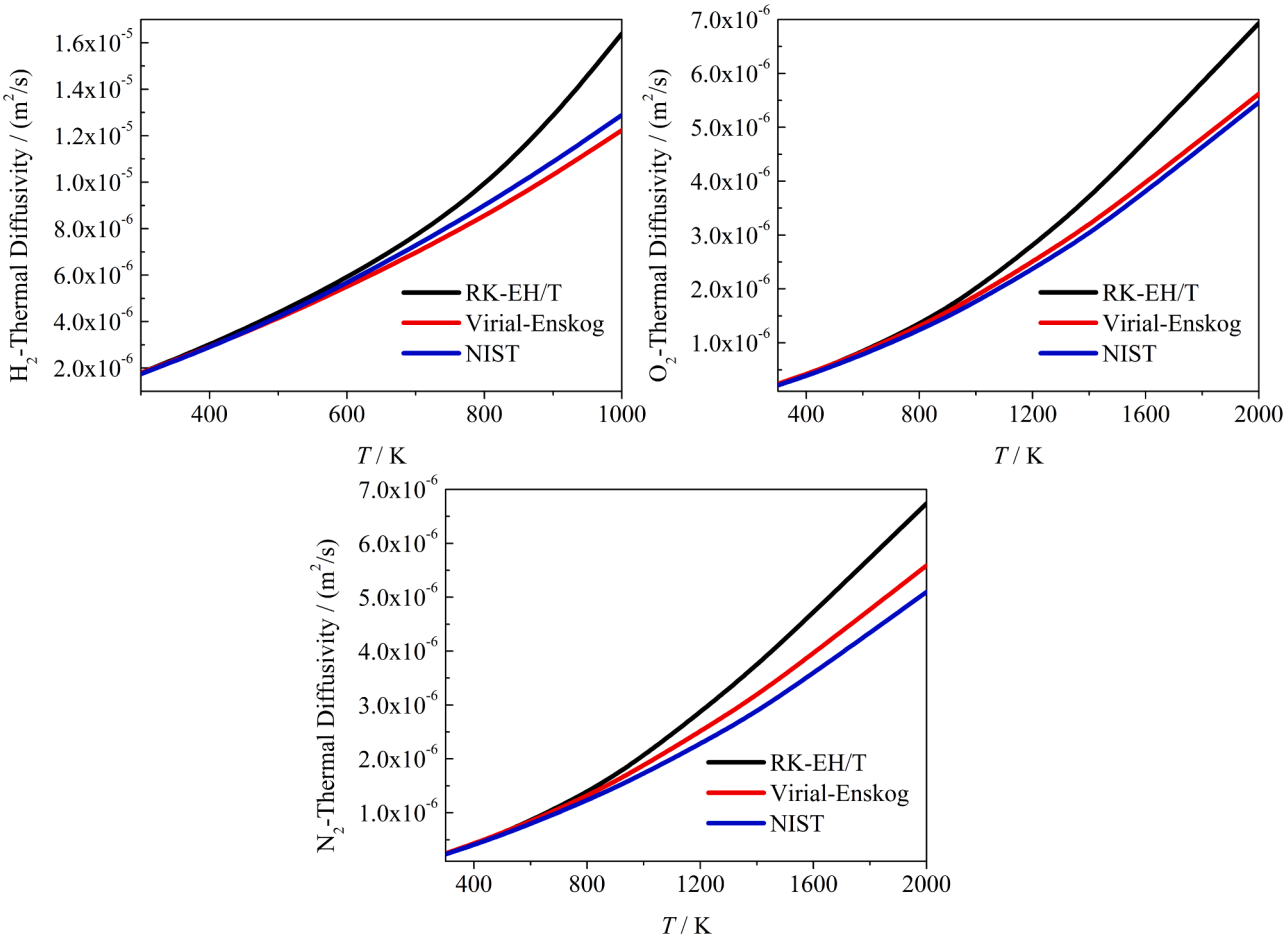


**Fig. 4.** The comparisons of the thermal diffusivities of hydrogen, nitrogen, oxygen, and methane at 100 atm computed by using different models with the NIST data [18].

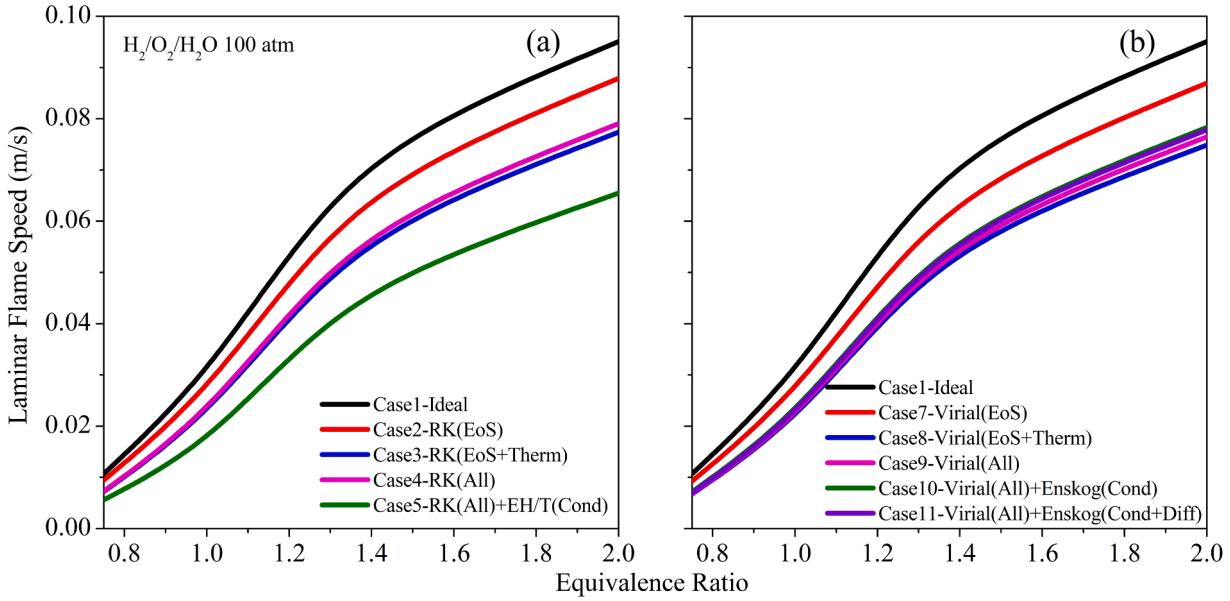


**Fig. 5.** The laminar flame speed simulations of $H_2/O_2/H_2O$ at 100 atm by using (a) the RK-EH/Takahashi and (b) the Virial-Enskog model. $T_i$=600K.

Fig. 7. It further indicates the weakness of the EH model in evaluating the real-fluid thermal conductivities of small molecules. The overall effects of real-fluid behaviors on the laminar flame speed simulations can reach 35 % at 100 atm according to Fig. 5. The effects of real-fluid thermal diffusivity $\lambda/\rho c_p$ shown in Fig. 6. are also significant. These all reveal that accurate descriptions of real-fluid effects are crucial for flame speed predictions, especially using dilute gas with strong real-fluid effects, such as $H_2O$.

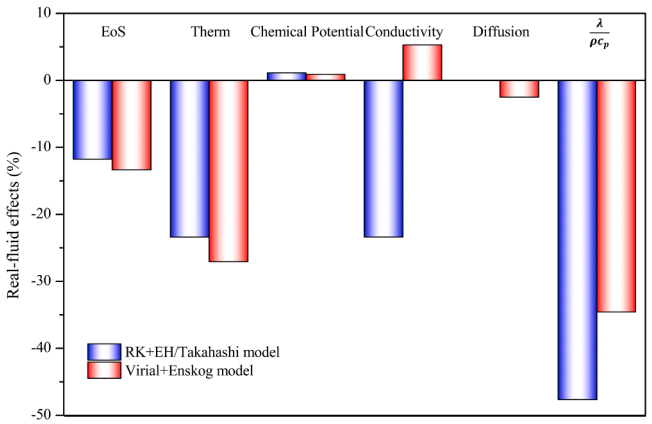


**Fig. 6.** The analyses of the real-fluid effects based on the laminar flame speed simulations of $H_2/O_2/H_2O$ at 100 atm by using the RK-EH/Takahashi and the Virial-Enskog model. $T_i$=600 K, φ=0.75.

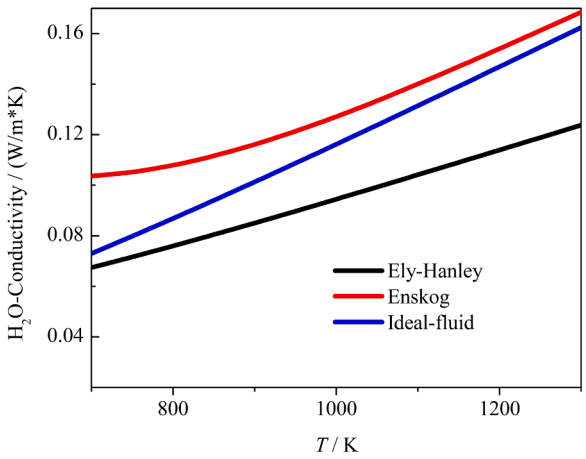


**Fig. 7.** The comparisons of the thermal conductivities of water computed by using different models at 100 atm.

### 3.2. Methane/air flames

The simulations of the methane laminar flame at 100 atm at different equivalence ratios are shown in Fig. 8. GRI-Mech [36] was used in the simulations. Different from Fig. 1, the laminar flame speeds decrease using the RK or the Virial EoS rather than using the ideal EoS. To explain this difference, the density of the mixture and the burning flux variation with the equivalence ratios using the ideal and Virial EoS for hydrogen and methane are shown in Fig. 9. The burning flux is almost unaffected by the Virial EoS in both hydrogen/air and methane/air system. However, the density of the real-fluid mixture is lower than the ideal gas in the hydrogen/air system, while it is larger in the methane/air system. It explains the arguments above. Similar to Fig. 1, considering the real-fluid thermodynamics, the reactivity of the system is inhibited and the laminar flame speeds are decreased in Case 3 and Case 8. From Cases 3 and 8 to Cases 4 and 9, considering the correction of the real-fluid chemical potential, species activity concentrations increase and correspond to the faster oxidation of methane in the real-fluid simulations. From Case 4 to Case 5, similar to Fig. 1, the laminar flame speeds increase using the EH model. It is noted that the prediction performance of the EH model is reasonably good for the methane/air flame simulations. This is because the correction of methane thermal conductivities in the EH model is directly from experimental measurement, resulting in a much lower uncertainty than the hydrogen flame simulations by using the EH model, where the thermal conductivities of hydrogen are from the principle of corresponding states. The thermal conductivities of methane computed by using both the EH and the Enskog models were compared with the NIST data and shown in Fig. 3. It can be observed that the thermal conductivities of methane computed by using both models show a good agreement with the NIST data. The EH model seems more accurate for thermal conductivity for methane as it is trained mainly from the methane transport experimental data. However, nitrogen and oxygen are also major components in the $CH_4$/air mixture. Hence, the large deviation of the EH model for nitrogen and oxygen will still cause large errors in predicting the laminar flame speeds. The simulation results computed using the Takahashi real-fluid mass diffusion model are not provided because of the convergence problem. Consistent with the hydrogen/air system, in Cases 10 and 11, the laminar flame speeds increase with the increase of the thermal conductivities in real dense fluids. The effects of mass diffusion corrections

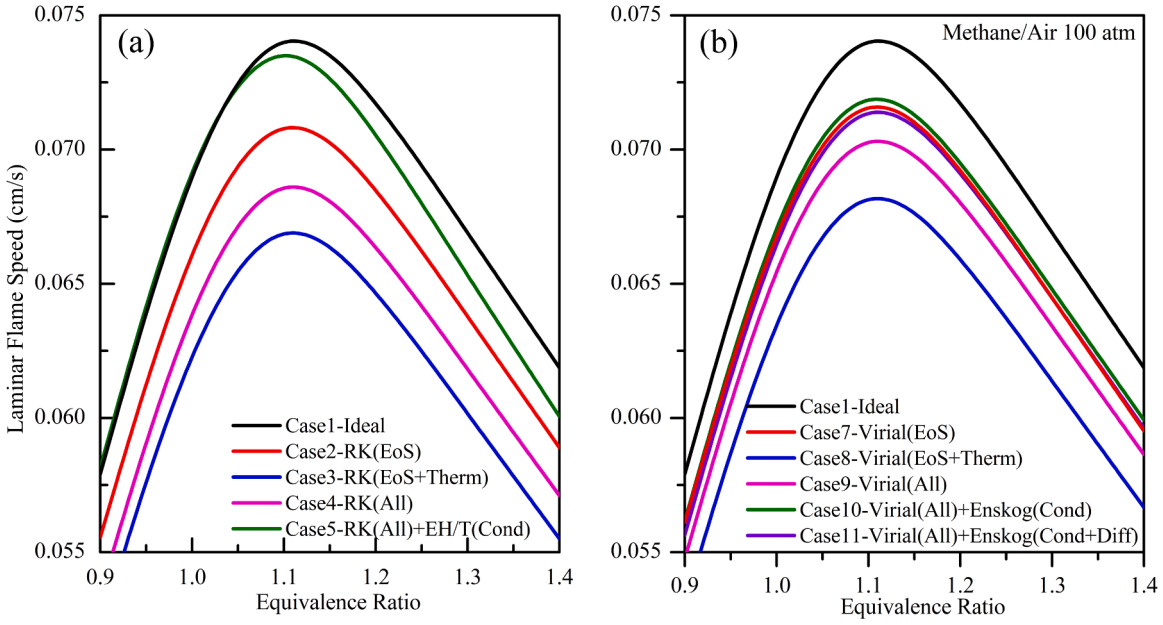


**Fig. 8.** The laminar flame speed simulations of methane/air at 100 atm by using (a) the RK-EH/Takahashi and (b) the Virial-Enskog model. $T_i$=298K.

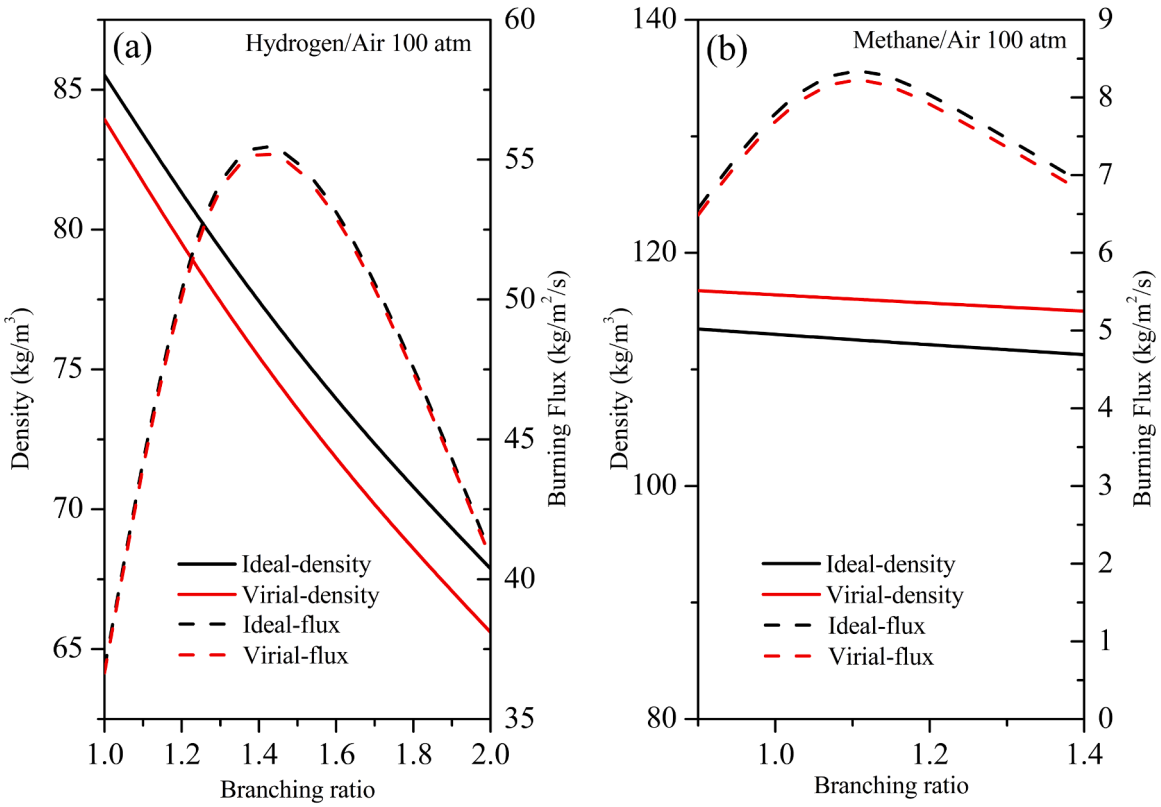


**Fig. 9.** Density and burning flux of hydrogen/air and methane/air at 100 atm using the ideal and Virial EoS.

are relatively small and simulated by using the Enskog model.

### 3.3. DME/air and n-heptane/air flames

The simulations of the dimethyl ether (DME) laminar flame and the n-heptane laminar flame at 100 atm at different equivalence ratios are shown in Figs. 10 and 11. The Sandiego mechanisms for DME [37] and n-heptane [38] were used in the simulations. For DME, the laminar flame speeds decrease using both real-fluid EoS compared with using the ideal EoS, due to the decrease of the density of the mixture in the DME/air system in Case 2 and Case 7. For n-heptane, the laminar flame speeds increase at lean-fuel conditions and decrease at rich-fuel conditions using both real-fluid EoS compared with using the ideal EoS. The reason is that the real-fluid densities of the n-heptane/air mixture decrease at lean-fuel conditions and increase at rich-fuel conditions. The effect trends are consistent with the simulation results in the methane/air system in other cases. The laminar flame speeds decrease considering complete real-fluid corrections using both models.

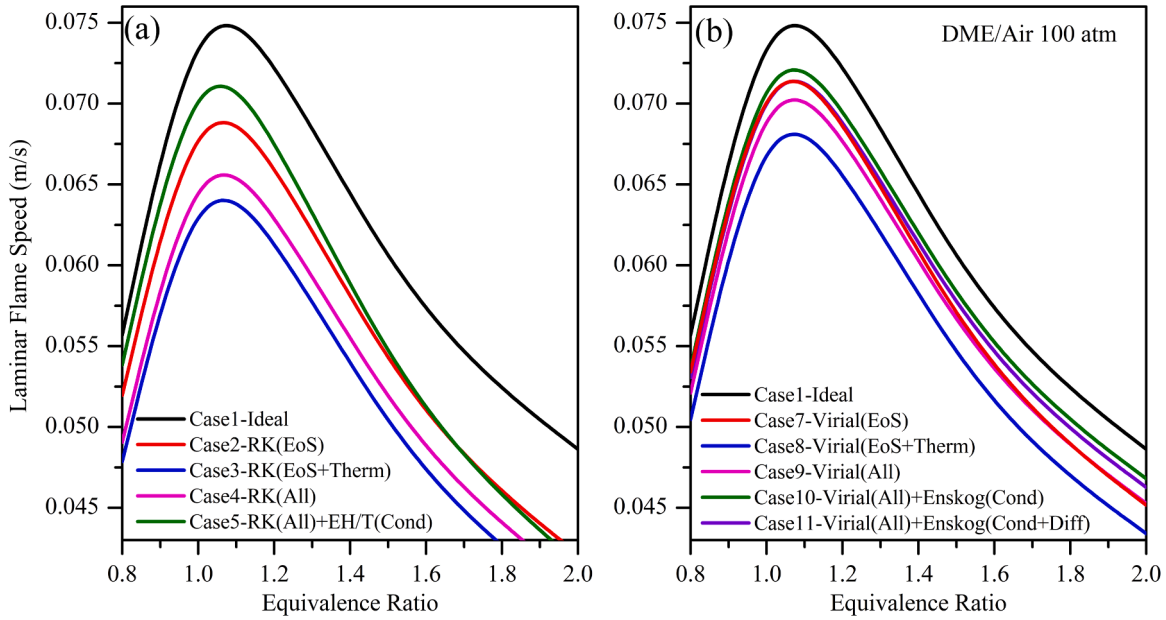


**Fig. 10.** The laminar flame speed simulations of DME/air at 100 atm by using (a) the RK-EH/Takahashi and (b) the Virial-Enskog model. $T_i$=298K.

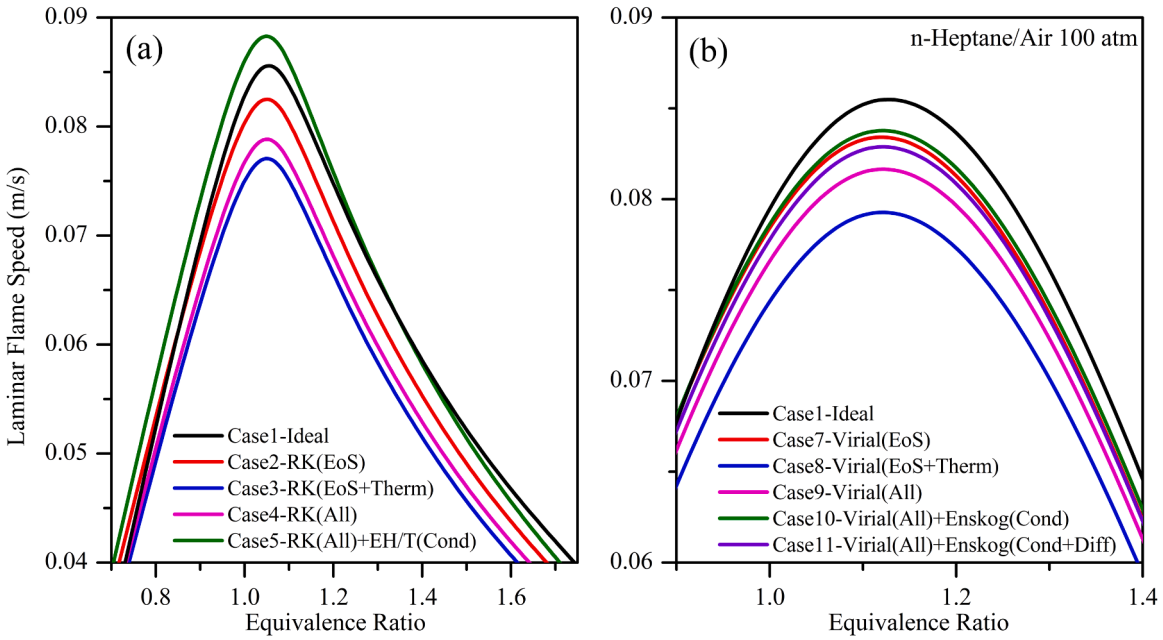


**Fig. 11.** The laminar flame speed simulations of n-heptane/air at 100 atm by using (a) the RK-EH/Takahashi and (b) the Virial-Enskog model. $T_i$=298K.

Moreover, in our simulations using the Virial-Enskog model for all fuels, we observe the increase of laminar flame speeds with including the real-fluid conductivities, which is opposite with the trends observed by Liang et al. [17] when adding thermal conductivity for $H_2$-air mixtures using the EH transport model. The predicted conductivities of $H_2$ and other relevant species with pressure and temperature from Cantera using the EH model are shown in Figs. S1 and S2, respectively. It shows that the thermal conductivities of $H_2$ and of other relevant species increase with pressure computed by using the EH model. These results are all consistent with our discussion as well as with the experimental results. The mixing rule and conformal mapping of the EH model were modified for the rich hydrogen/air mixtures to avoid significant over-predictions of the flame speeds in Liang et al.'s work, as such it leads to an decrease of the real-fluid $H_2$ conductivity in their computation.

The real-fluid effects for the different fuels at different equivalence ratio in air at 100 atm are shown in Table 1. The largest difference could reach to 7.5 %.

The comparisons of the laminar flame speed simulations for $H_2$—CO—$O_2$—He mixtures with the experimental data at 40 atm [39] are shown in Fig. 12. The GRI-MECH 3.0 [40] is used for simulations. The Virial-Enskog model predicts the smaller flame speeds than the ideal gas model. However, both the ideal-gas and the Virial-Enskog models could not capture the experimental data well. This indicates that the GRI-MECH may not be a very accurate mechanism to study flame speed in high-pressure CO—$H_2$ mixtures. Moreover, the real-fluid effect on kinetics is significant for future investigation.

**Table 1**
The real-fluid effects for the different fuels at different equivalence ratio in air at 100 atm. The value is the ratio of the flame speed calculated by using the Virial-Enskog model with using the ideal-gas model.

| Equivalence ratio | 0.7 | 0.9 | 1 | 1.2 | 1.5 | 1.75 | 2 |
|---|---|---|---|---|---|---|---|
| $H_2$ | – | – | 100.5 % | – | 102.0 % | 102.8 % | 103.2 % |
| $CH_4$ | – | 96.1 % | 96.4 % | 96.3 % | – | – | – |
| DME | – | – | 95.5 % | 95.2 % | 95.3 % | 95.3 % | 95.1 % |
| Heptane | 107.5 % | 99.2 % | 98.0 % | – | 96.4 % | 96.4 % | – |

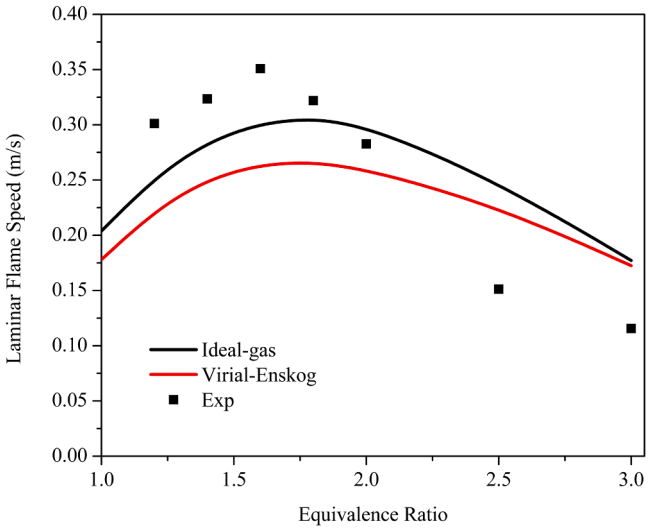


**Fig. 12.** The comparisons of the laminar flame speed simulations for the CO/$H_2$/He/$O_2$ flame with experimental data. The initial temperature and pressure are 298 K and 40 atm. The mixture composition is defined through $0.95CO+0.05H_2+(1/\varphi)(0.5O_2+3.5He)$ for CO/$H_2$/$O_2$/He.

The comparisons of the laminar flame speed simulations for the DME/$O_2$/$N_2$/He/$CO_2$ flame as a function of pressures with experimental data [41] are shown in Fig. 13. The initial temperature and the equivalence ratio are 295 K and 0.8. The Sandiego mechanism for DME [37] with 63 species and 284 reactions has been reduced to 24 species and 88 reactions to decrease real-fluid computational cost. The simulations with and without $CO_2$ dilution considering real-fluid behaviors by using the Virial-Enskog model were performed by using the reduced Sandiego mechanism. Both the Sandiego mechanism and the reduced Sandiego mechanism overestimate the laminar flame speeds. The laminar flame speeds decrease and the results are closer to experimental data considering real-fluid behaviors by using the Virial-Enskog model with and without $CO_2$ dilution, especially at higher pressures. The difference

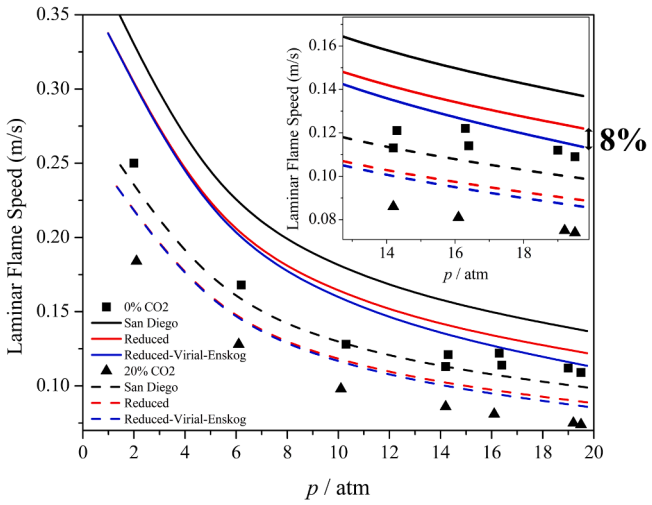


**Fig. 13.** The comparisons of the laminar flame speed simulations for the DME/$O_2$/$N_2$/He/$CO_2$ flame with experimental data [41]. The initial temperature and the equivalence ratio are 295 K and 0.8.

could reach 8 % even at only 20 atm.

The comparisons of the laminar flame speed simulations for the n-heptane/air flame as a function of equivalence ratios with experimental data [42] are shown in Fig. 14. The initial pressure and temperature are 25 atm and 373 K. The Sandiego mechanism for n-heptane [38] with 63 species and 284 reactions has been reduced to 24 species and 88 reactions to decrease real-fluid computational cost. The simulations considering real-fluid behaviors by using the Virial-Enskog model were performed using the reduced Sandiego mechanism. The laminar flame speeds increase considering real-fluid behaviors and the difference could reach 6 % at only 25 atm. It is noticed that the Virial-Enskog model predicts the smaller flame velocities than the ideal gas EoS model at rich-fuel conditions in Fig. 9 but the higher values at lean-fuel conditions in Fig. 11 for heptane. That is due to a higher contribution of real-fluid thermal conductivities at lean-fuel conditions in Fig. 9.

Therefore, the real-fluid effects are significant on the laminar flame propagations in supercritical mixtures according to our simulations. The Virial-Enskog model can provide a better description of the effects of

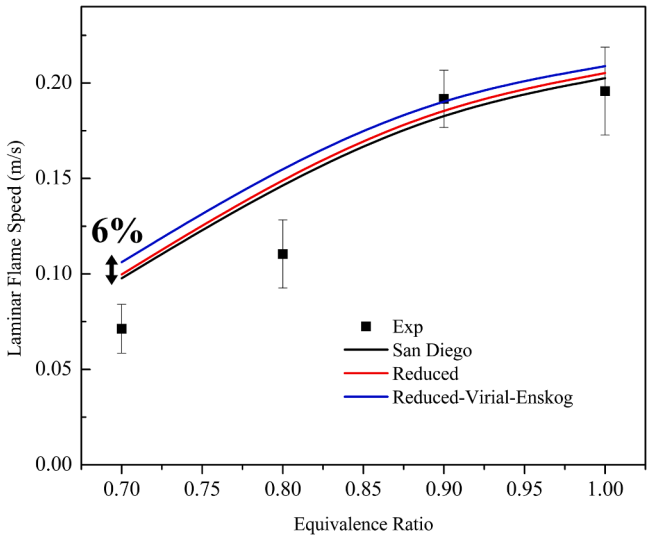


**Fig. 14.** The comparisons of the laminar flame speed simulations for the n-heptane/air flame with experimental data [42]. The initial pressure and temperature are 25 atm and 373 K.

real-fluid behaviors based on its accurate prediction of real-fluid EoS, thermodynamics, chemical potential, thermal conductivities, and mass diffusions. More high-pressure laminar flame speed experiments will be helpful to the further validation of the Virial-Enskog model. The predictions of laminar flame speed for other fuels are also highly dependent on their kinetic mechanisms. The real-fluid effect on kinetics is also very important and complicated, which needs considerations of multi-body collisions and non-negligible intermolecular force. It will be one of our future work.

The computational cost mainly relies on the real-fluid model and the size of mechanism, and it varies with the difficulties of convergence. The computational cost for the Virial-Enskog model is about a factor of 5 higher than the RK-EH/Takahashi model for hydrogen, about a factor of 10 higher for methane, about a factor of 20 higher for DME and heptane which mainly from the calculation cost of the Virial EoS. Even though the computational cost is larger now, the machine learning method will be incorporated to reduce the circulation in codes by about a factor of 2–5 in our future work.

## 4. Conclusion

In this work, both the EH/Takahashi model and the Enskog model were developed to account for the real-fluid effects on transport properties under supercritical conditions. The calculations of real-fluid transport properties have been coupled with the calculations of the real-fluid EoS, thermodynamics properties, and chemical potentials to realize the real-fluid laminar flame simulations under supercritical conditions.

The real-fluid effects on compressibility factors, thermodynamic properties, chemical potentials, and transport properties for the laminar flame simulations in the supercritical hydrogen/air, $H_2/O_2/H_2O$, methane/air, DME/air, n-heptane/air mixtures have been discussed respectively. The contribution and the source of uncertainties by different real-fluid properties are also comprehensively discussed. The overall effects of real-fluid behaviors on the laminar flame speed simulations in $H_2O$ can reach 35 % at 100 atm, which reveal that accurate descriptions of real-fluid effects are crucial for flame speed predictions, especially using dilute gas with a high polarization, such as $H_2O$. The RK-EH/Takahashi model shows severe over-predictions of the hydrogen laminar flame speeds, due to the significant weakness in predictions of thermal conductivities of mixtures by comparing with the NIST data, while the present Virial-Enskog model exhibits more reasonable predictability. The effects of the real-fluid mass diffusions are relatively small because only within ±10 % deviation of mass diffusions are caused by real-fluid behaviors.

The laminar flame speed results for DME and n-heptane flame simulated by using the real-fluid models were also compared with the experimental data in the literature. The laminar flame speeds for the DME/$O_2$/$N_2$/He/$CO_2$ flame decrease and the results are closer to experimental data considering real-fluid behaviors by using the Virial-Enskog model, especially at higher pressures. It shows a crucial real-fluid effect on the simulations of DME and n-heptane flame speeds, up to 8 % discrepancy from the ideal-gas flame speed prediction, even at 20–25 atm. Overall, the Virial-Enskog model provides better estimations of the real-fluid behaviors than the empirical RK-EH/Takahashi model, especially at high pressures.

## CRediT authorship contribution statement

**Junfeng Bai:** Writing – original draft, Validation, Software, Methodology, Investigation, Conceptualization. **Xin Zhang:** Methodology, Conceptualization. **Hao Zhao:** Writing – review & editing, Supervision, Methodology, Conceptualization.

## Declaration of interest statement

The authors declare that they have no known competing financial interests or personal relationships that could have appeared to influence the work reported in this paper.

*Acknowledgments*

This work was supported by the National Natural Science Foundation of China (no. 22361132538, no. 22350710788), the Fund of Ministry of Education (no. 8091B032244), the Open Fund of the State Key Laboratory of Engines of China (no. K2023-11), the Open Fund of the Ministry Key Laboratory of Marine Power Engineering and Transport Technology (no. KLMPET2022-01), and the Space Power Fund of the China Space Foundation (No. KDJJ20230202005).

## Supplementary materials

Supplementary material associated with this article can be found, in the online version, at doi:10.1016/j.combustflame.2025.114144.

## References

[1] M. Li, H. Wu, T. Zhang, B. Shen, Q. Zhang, Z. Li, A comprehensive review of pilot ignited high pressure direct injection natural gas engines: factors affecting combustion, emissions and performance, Renew. Sust. Energ. Rev. 119 (2020) 109653.
[2] S.M. Correa, A review of NOx formation under gas-turbine combustion conditions, Combust. Sci. Technol. 87 (1993) 329–362.
[3] J.C. Oefelein, V. Yang, Modeling high-pressure mixing and combustion processes in liquid rocket engines, J. Propul. Power 14 (1998) 843–857.
[4] H. Zhao, C. Yan, T. Zhang, G. Ma, M.J. Souza, C.-W. Zhou, Y. Ju, Studies of high-pressure n-butane oxidation with $CO_2$ dilution up to 100 atm using a supercritical-pressure jet-stirred reactor, Proc. Combust. Inst. 38 (2021) 279–287.
[5] R. Payri, F. Salvador, J. Gimeno, G. Bracho, The effect of temperature and pressure on thermodynamic properties of diesel and biodiesel fuels, Fuel 90 (2011) 1172–1180.
[6] A. Burcat, Thermochemical Data For Combustion calculations, Combustion Chemistry, Springer, 1984, pp. 455–473.
[7] N. Sakoda, K. Shindo, K. Shinzato, M. Kohno, Y. Takata, M. Fujii, Review of the thermodynamic properties of hydrogen based on existing equations of state, Int. J. Thermophys. 31 (2010) 276–296.
[8] J. Bai, P. Zhang, C.-W. Zhou, H. Zhao, Theoretical studies of real-fluid oxidation of hydrogen under supercritical conditions by using the virial equation of state, Combust. Flame 243 (2022) 111945.
[9] J. Bai, X. Zhang, C.-W. Zhou, P. Zhang, H. Zhao, Theoretical studies of supercritical real-fluid oxidations of diverse fuels by using the 3rd-order virial equation of state with nonlinear effects, Combust. Flame 270 (2024).
[10] K.S. Pitzer, R. Curl Jr, The volumetric and thermodynamic properties of fluids.: III. Empirical equation for the second virial coefficient, molecular structure and statistical thermodynamics: selected papers of Kenneth S Pitzer, World Scientif. (1993) 311–312.
[11] O. Redlich, J.N. Kwong, On the thermodynamics of solutions. V. An equation of state. Fugacities of gaseous solutions, Chem. Rev. 44 (1949) 233–244.
[12] S. Chapman, T. Cowling, Press, 1939.
[13] J.O. Hirschfelder, C.F. Curtiss, R.B. Bird, M.G. Mayer, Molecular Theory of Gases and Liquids, Wiley, New York, 1964.
[14] J.G. Kirkwood, The statistical mechanical theory of transport processes I. General theory, J. Chem. Phys. 14 (1946) 180–201.
[15] J.F. Ely, H.J.M. Hanley, Prediction of transport properties. 2. Thermal conductivity of pure fluids and mixtures, Ind. Eng. Chem. Fundam. 22 (1983) 90–97.
[16] S. Takahashi, Preparation of a generalized chart for the diffusion coefficients of gases at high pressures, J. Chem. Eng. Jpn. 7 (1975) 417–420.
[17] W. Liang, W. Li, C.K. Law, Laminar flame propagation in supercritical hydrogen/air and methane/air mixtures, Proc. Combust. Inst. 37 (2019) 1733–1739.
[18] P. Linstorm, NIST chemistry webbook, NIST standard reference database number 69, J. Phys. Chem. Ref. Data Monogr. 9 (1998) 1–1951.
[19] C.K. Law, Combustion Physics, Cambridge university press, 2010.
[20] A. Gopal, P.S. Volpiani, S. Yellapantula, J. Larsson, Computational investigation of real fluid effects in cryogenic laminar premixed $CH_4$–$O_2$ flames, J. Supercrit. Fluid. 168 (2021) 105045.
[21] T.H. Chung, M. Ajlan, L.L. Lee, K.E. Starling, Generalized multiparameter correlation for nonpolar and polar fluid transport properties, Ind. Eng. Chem. Res. 27 (1988) 671–679.
[22] H. Terashima, M. Koshi, Prediction of propagating flames under high-pressure conditions with real-fluid combustion modeling, Proc. Combust. Inst. 39 (2023) 1823–1831.
[23] M.R. Riazi, C.H. Whitson, Estimating diffusion coefficients of dense fluids, Ind. Eng. Chem. Res. 32 (1993) 3081–3088.
[24] V. Giovangigli, L. Matuszewski, F. Dupoirieux, Detailed modeling of planar transcritical $H_2$–$O_2$–$N_2$flames, Combust. Theory Model. 15 (2011) 141–182.
[25] Z. Weng, Y. Zhang, B.M. Maxwell, R. Mével, The effect of finite molecular volume on the propagation of unsteady spherical flame front, Combust. Flame 263 (2024).
[26] Y. Zhang, Z. Weng, R. Mével, Laminar flame speeds of supercritical $CO_2$ diluted oxy-syngas and oxy-methane flames under direct-fired power cycle relevant conditions, Combust. Flame 266 (2024).
[27] Z. Lv, H. Cao, W. Han, L. Yang, Real-fluid effects on laminar premixed hydrogen flames under cryogenic and high-pressure conditions, Combust. Flame 272 (2025).
[28] D.G. Goodwin, R.L. Speth, H.K. Moffat, B.W. Weber, Cantera: An Object-Oriented Software Toolkit for Chemical Kinetics, Thermodynamics, and Transport Processes, 2018. https://www.cantera.org.
[29] R.B. Bird, E.L. Spotz, J. Hirschfelder, The third virial coefficient for non-polar gases, J. Chem. Phys. 18 (1950) 1395–1402.
[30] J.E. Lennard-Jones, On the determination of molecular fields. II. From the equation of state of gas, Proc. Roy. Soc. A 106 (1924) 463–477.
[31] W.H. Stockmayer, Second virial coefficients of polar gases, J. Chem. Phys. 9 (1941) 398–402.
[32] J. Rowlinson, The second virial coefficients of polar gases, Trans. Faraday Soc. 45 (1949) 974–984.
[33] G. Kogekar, C. Karakaya, G.J. Liskovich, M.A. Oehlschlaeger, S.C. DeCaluwe, R. J. Kee, Impact of non-ideal behavior on ignition delay and chemical kinetics in high-pressure shock tube reactors, Combust. Flame 189 (2018) 1–11.
[34] G.-N. Dixon-Lewis, Flame structure and flame reaction kinetics II. Transport phenomena in multicomponent systems, Proceed. Roy. Soc. Lond. Ser A. Math. Phys. Sci. 307 (1968) 111–135.
[35] M.P. Burke, M. Chaos, Y. Ju, F.L. Dryer, S.J. Klippenstein, Comprehensive $H_2/O_2$ kinetic model for high-pressure combustion, Int. J. Chem. Kinet. 44 (2012) 444–474.
[36] G.P. Smith, GRI-Mech 3.0, 1999. http://www.me.berkley.edu/gri_mech/.
[37] J.C. Prince, F.A. Williams, A short reaction mechanism for the combustion of dimethyl-ether, Combust. Flame 162 (2015) 3589–3595.
[38] T.J. Held, A.J. Marchese, F.L. Dryer, A semi-empirical reaction mechanism for n-heptane oxidation and pyrolysis, Combust. Sci. Technol. 123 (1997) 107–146.
[39] H. Sun, S.I. Yang, G. Jomaas, C.K. Law, High-pressure laminar flame speeds and kinetic modeling of carbon monoxide/hydrogen combustion, Proc. Combust. Inst. 31 (2007) 439–446.
[40] G.P. Smith, GRI-Mech 3.0, 1999. http://www.me.berkley.edu/gri_mech/.
[41] D. Liu, J. Santner, C. Togbé, D. Felsmann, J. Koppmann, A. Lackner, X. Yang, X. Shen, Y. Ju, K. Kohse-Höinghaus, Flame structure and kinetic studies of carbon dioxide-diluted dimethyl ether flames at reduced and elevated pressures, Combust. Flame 160 (2013) 2654–2668.
[42] S. Jerzembeck, N. Peters, P. Pepiotdesjardins, H. Pitsch, Laminar burning velocities at high pressure for primary reference fuels and gasoline: experimental and numerical investigation, Combust. Flame 156 (2009) 292–301.